Combustion Theory and Modelling
Vol. 12, No. 5, October 2008, 857–882

Taylor & Francis
Taylor & Francis Group

Lagrangian investigation of local extinction, re-ignition and auto-ignition in turbulent flames

Haifeng Wang* and Stephen B. Pope

Sibley School of Mechanical and Aerospace Engineering, Cornell University, Ithaca, NY 14853, USA

(*Received 15 April 2007*)

Lagrangian PDF investigations are performed of the Sandia piloted flame E and the Cabra H_2/N_2 lifted flame to help develop a deeper understanding of local extinction, re-ignition and auto-ignition in these flames, and of the PDF models' abilities to represent these phenomena. Lagrangian particle time series are extracted from the PDF model calculations and are analyzed. In the analysis of the results for flame E, the particle trajectories are divided into two groups: continuous burning and local extinction. For each group, the trajectories are further sub-divided based on the particles' origin: the fuel stream, the oxidizer stream, the pilot stream, and the intermediate region. The PDF calculations are performed using each of three commonly used models of molecular mixing, namely the EMST, IEM and modified Curl mixing models. The calculations with different mixing models reproduce the local extinction and re-ignition processes observed in flame E reasonably well. The particle behavior produced by the IEM and modified Curl models is different from that produced by the EMST model, i.e., the temperature drops prior to (and sometimes during) re-ignition. Two different re-ignition mechanisms are identified for flame E: auto-ignition and mixing-reaction. In the Cabra H_2/N_2 lifted flame, the particle trajectories are divided into different categories based on the particles' origin: the fuel stream, the oxidizer stream, and the intermediate region. The calculations reproduce the whole auto-ignition process reasonably well for the Cabra flame. Four stages of combustion in the Cabra flame are identified in the calculations by the different mixing models, i.e., pure mixing, auto-ignition, mixing-ignition, and fully burnt, although the individual particle behavior by the IEM and modified Curl models is different from that by the EMST model. The relative importance of mixing and reaction during re-ignition and auto-ignition are quantified for the IEM model.

Keywords: PDF method, particle tracking, particle trajectories, mixing models, local extinction, re-ignition, auto-ignition

1. Introduction

Flame extinction and ignition are fundamental phenomena in combustion problems. The occurrence of extinction and ignition in turbulent reactive flows, due to intensive non-linear turbulence-chemistry interactions, is a challenge to modern turbulent combustion models. The probability density function (PDF) transport equation method [1–3] is increasingly found to be able to account accurately for the turbulence-chemistry interactions, e.g., local extinction and re-ignition [4, 5]. In engineering practice, the statistics of the turbulent velocity and composition fields are of primary concern in the context of Reynolds averaged Navier–Stokes (RANS) simulations. In PDF methods, the modeled PDF transport equation is usually solved numerically by a Lagrangian

*Corresponding author. Email: hw98@cornell.edu

ISSN: 1364-7830 print / 1741-3559 online

DOI: 10.1080/13647830802056137
http://www.tandf.co.uk/journals

particle method, and much more information can be extracted from the particle properties. Particle scatter plots (or joint PDFs) contain the most detailed information about the distribution of properties at a given position and time. All previous PDF calculations of turbulent flames have focused on Eulerian statistics and their comparison with experimental data, e.g., conditional or unconditional statistics of compositions, particle scatter plots and conditional PDFs of compositions. Scatter plots of particle properties are able to illustrate qualitatively different kinds of complicated turbulent combustion phenomena such as local extinction and re-ignition. To explore the PDF calculation results comprehensively, and to understand the turbulence-chemistry interactions more deeply, here we extract and analyze Lagrangian time series of particle properties from the PDF calculations. The particle trajectories are presented to illustrate the dynamic evolution of complicated turbulent combustion processes, i.e., local extinction and re-ignition in the turbulent non-premixed piloted jet flame, and auto-ignition in the turbulent lifted jet flame.

Lagrangian properties are important physical properties relevant not only to the PDF method, but also to real turbulence and combustion problems. Many Lagrangian investigations have been performed of turbulence using direct numerical simulations (DNS). Yeung [6, 7] studied the Lagrangian characteristics of turbulence and passive scalar transport in stationary isotropic turbulence with uniform mean scalar gradients. The Lagrangian properties of the scalars investigated are important to molecular mixing models. Mitarai *et al*. [8] performed DNS of an idealized non-premixed flame in decaying isotropic turbulence for conditions where flame extinction and re-ignition occur. In that work, the fluid particles are tracked to investigate flame extinction and re-ignition. Different categories of particles are identified, e.g., continuous burning and local extinction. Also investigated are Lagrangian properties of the conditional scalar diffusion, which appears as an unclosed term in the PDF transport equation. The same methodology is used to investigate the performance of flamelet models [9] and the performance of different mixing models [10]. Sripakagorn *et al*. [11] performed Lagrangian flame element tracking along the stoichiometric surface in decaying isotropic turbulence to investigate flame extinction and re-ignition. Three major scenarios of re-ignition in non-premixed combustion are identified, i.e., the independent flamelet scenario, re-ignition via edge flame propagation, and re-ignition through engulfment by hot neighbouring fluid. These Lagrangian investigations are helpful to provide insights into the dynamic evolution of turbulent combustion processes. Because of the formidable practical difficulties there are no experimental data on Lagrangian quantities in turbulent reactive flows. Experimental data are, however, becoming available on Lagrangian velocity and acceleration statistics in non-reactive flows [12–14].

The Lagrangian PDF method [2] represents the turbulent flow, transport and reaction processes via the time evolution of nominal Monte Carlo particles representing the joint PDF of velocity, turbulence frequency and compositions. Eulerian statistics obtained from PDF calculations have been explored extensively before, and are generally found to be in good agreement with the experimental data. It would be valuable to extract the Lagrangian time series which contains the whole history of the particle evolution in the multi-dimensional sample space. This work is dedicated, as a first effort, to explore the Lagrangian properties of the Monte Carlo particles in the PDF simulations of turbulent flames containing local extinction and re-ignition, and auto-ignition. The two flames studied are the Sandia non-premixed piloted jet flame E [15], and the lifted H_2/N_2 jet flame in a vitiated coflow [16], referred to as the Cabra flame.

In PDF methods, the closed form of the chemical reaction source term facilitates the exact treatment of detailed combustion chemistry. The modeling of the unclosed molecular mixing term in the PDF equation remains one of the major efforts of model development. Three mixing models are extensively used, i.e. the Euclidean minimum spanning tree (EMST) model [21], the interaction by exchange with the mean (IEM) model [18] (or the least-mean-square estimator

(LMSE) model [19]), and the modified Curl model [20, 22]. All the mixing models can represent local extinction and re-ignition to some extent [4, 5, 23], although the EMST model is usually thought to be superior in this respect. The simplicity of the IEM and modified Curl models makes them quite popular. In spite of the complexity of the EMST model, the public availability of a FORTRAN implementation [24] makes it easy to use. A desirable property of mixing models is "localness" [21]. All the models are local in physical space; only the EMST model is local in composition space; and none is local in velocity space. There is some recent progress in the development of more sophisticated mixing models, e.g., the multiple mapping conditioning (MMC) model [25],and the interaction by exchange with the conditional mean (IECM) mixing model [26–29], which is local in velocity space. The present work focuses on the three traditional mixing models (EMST, IEM and modified Curl) and evaluates their relative performance from the Lagrangian viewpoint.

The primary aim of PDF methods is to calculate accurately one-point, one-time Eulerian quantities. It is well understood [1] that this objective can be achieved using stochastic Lagrangian models, even if the multi-time properties of the models are not physically accurate. While the multi-time behavior of the stochastic models for position and velocity are physically realistic, those of the mixing models are not. For example Curl's model involves jumps in compositions; and (for the simplest homogeneous turbulence) the IEM model yields a deterministic relaxation to the mean, with no fluctuations along Lagrangian trajectories. Hence, while this study is valuable in shedding light on the models' behavior and performance, a close correspondence between the models' Lagrangian trajectories and those in the flame (could they be measured!) should not be expected.

The remaining sections of this paper are organized as follows. In Section 2, Eulerian scatter plots of particle properties are presented for the Sandia piloted flame E [15] and for the Cabra H_2/N_2 lifted jet flame [16]. The illustrations of local extinction and re-ignition, and of auto-ignition are reviewed by reference to the Eulerian particle data. The limitations of the Eulerian data are discussed. In Section 3, the particle tracking and particle sampling procedures are presented. In Sections 4 and 5 (for the Sandia flame E and the Cabra lifted flame, respectively), the Lagrangian time series obtained from the PDF calculation using the different mixing models are analyzed to study the models' representation of extinction, re-ignition and auto-ignition. The relative roles of mixing and reaction during re-ignition and auto-ignition are quantified for the IEM model in Section 6. Conclusions are drawn in the final section.

2. Particle calculations and Eulerian scatter plots

Comprehensive PDF model investigations of the Sandia piloted flames and the Cabra H_2/N_2 lifted jet flame have been described elsewhere [4, 5, 16, 23, 30–32]. In this section, PDF calculations of the Sandia flame E and the Cabra lifted jet flame are repeated to review the Eulerian particle scatter plots. As in [23, 30], a PDF code called HYB2D is used, in which a hybrid finite volume (FV)/particle algorithm is implemented for solving the joint PDF transport equation of the velocity, turbulence frequency and compositions [34]. The details of the simulations for the Sandia flame E and the Cabra lifted jet flame are identical to those in [35] and in [31], respectively, and are simply summarized in Table 1. (Quantities not listed in Table 1 can be found in [31] and [35].) Different values of the mixing model constant C_ϕ are specified for the different mixing models in the calculation of the Sandia flame E in order to achieve a stable burning flame with roughly the same amount of local extinction [23, 35] as observed experimentally. Similarly, different coflow temperatures are used in the calculation of the Cabra lifted flame with different mixing models in order to produce approximately the same flame lift-off height as observed experimentally [31].

Table 1. Details of the simulations for the Sandia flame E and the Cabra lifted H_2/N_2 jet flame.

Model parameters	Sandia flame E			Cabra lifted flame		
Turbulence frequency model constant [17], $C_{\omega 1}$	0.7			0.65		
Number of particles per cell, N_{pc}	100			100		
Chemistry	GRI-Mech 3.0 [37]			H_2-O_2 mechanism [38]		
ISAT error tolerance [36], ε_{tol}	5.0×10^{-5}			6.25×10^{-6}		
Grid size	96×96			96×96		
	EMST	IEM	modified Curl	EMST	IEM	modified Curl
Mixing model constant, C_ϕ	1.5	2.7	3.3	1.5	1.5	1.5
Coflow temperature in Cabra lifted flame, T_c(K)	—	—	—	1033	1036	1036

Conventionally, the output from PDF calculations is Eulerian data for analysis at a fixed time (when the statistically stationary state has been reached) and at different locations. The conditional and unconditional statistics of the Eulerian data have been discussed extensively elsewhere [4, 5, 23, 30, 31] and will not be repeated here. In this section, we review the scatter plots of the particle temperature versus the mixture fraction in the Sandia flame E and the Cabra lifted flame. As previously discussed [4], it is difficult to make a rigorous quantitative comparison between scatter plots from experiment and model calculations, because of differences in the sampling and weighting of particles. Nevertheless, this comparison is useful in assessing, at least qualitatively, the ability of the models to represent the phenomena observed experimentally.

Figure 1 shows the scatter plots of the particle temperature against the mixture fraction at different axial locations in the Sandia flame E from measurements [15], and from the PDF simulations with different mixing models. The axial distance x is shown as x/D, where D is the diameter of the fuel jet. Two laminar flame temperature profiles (dashed lines in Figure 1) are also shown for reference. The laminar calculations are conducted by using OPPDIF [39] with two strain rates, $a = 10\ \text{s}^{-1}$ and $310\ \text{s}^{-1}$, and in the latter case, the temperature profile is shifted down by 300 K. Following [8], we use this shifted temperature profiles with a =310 s^{-1} as a simple criterion to distinguish between burning particles (above the line) and extinguished particles (below the line). For simplicity, we call this line the "extinction line", and the region above the "burning region", and the region below the "extinction region". There is of course an extinction limit of strain rate a_e ($a_e \approx 376\ \text{s}^{-1}$ for the current case) and its corresponding temperature profile in steady opposed laminar non-premixed jet flames, but we prefer not to use this extinction limit as our criterion. The extinction limit a_e applies only to steady laminar flames. In the unsteady case (e.g., laminar flames subject to the oscillation of strain rate), however, the instantaneous strain rate can exceed the extinction limit, without the flame being extinguished [40, 41]. Using the extinction limit of the steady laminar flame will somewhat over-estimate the amount of local extinction in this turbulent flame. Hence, as in [8], we use the shifted temperature profiles as a more conservative extinction limit. This criterion is somewhat arbitrary, but it is helpful for the qualitative analysis of the local extinction and re-ignition reported below.

From the experimental scatter plots in Figure 1, it may be seen that the number of the particles below the extinction lines decreases with increasing the axial distance from $x/D = 7.5$ to 45, indicating the evolution from local extinction to re-ignition. The PDF calculations with the three mixing models qualitatively reproduce this process to some extent. The scatter plots of the Eulerian particle data visually illustrate the level of local extinction at different locations. However, the Lagrangian evolution of the particle properties is not evident. Where do the locally

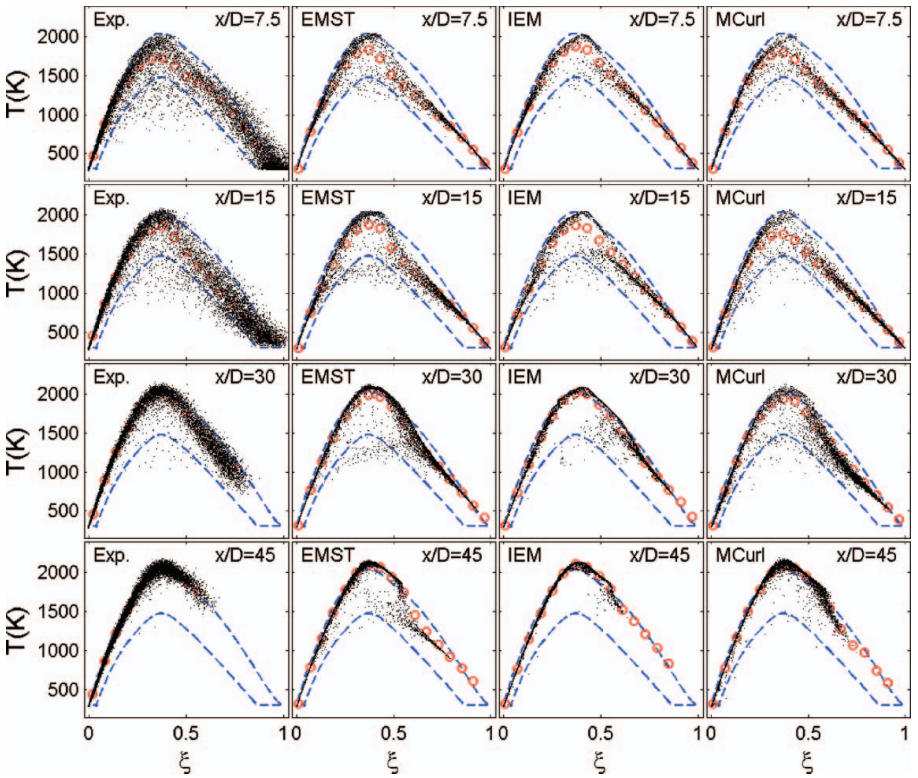

Figure 1. Scatter plots of temperature against the mixture fraction at the axial locations $x/D = 7.5$, 15, 30, and 45 in the Sandia piloted flame E from experimental data and from PDF calculations using three different mixing models (Open circles: conditional mean temperature; Dashed lines: temperature profiles in the opposed-jet laminar flame with strain rate $a = 10\text{s}^{-1}$ (upper lines); and with strain rate $a = 310\text{s}^{-1}$ (lower lines), shifted down by 300 K.)

extinguished particles come from? How do they return to the burning region (in composition space)? How do different mixing models cause the particles to move in the composition space? The current Eulerian data cannot answer these questions.

We now turn our attention to the Cabra H_2/N_2 lifted jet flame. Figure 2 shows the scatter plots of temperature versus mixture fraction at different axial locations in the flame. The equilibrium state calculated by using EQUIL [42] is also shown in the plots for reference. The initial enthalpy h and the species mass fractions $\mathbf{Y}$ for the equilibrium calculation are taken to be linear in the mixture fraction ξ space, i.e.

$$h(\xi) = h_{\text{ox}} - (h_{\text{ox}} - h_{\text{fu}}) \cdot \xi \tag{1}$$

$$\mathbf{Y}(\xi) = \mathbf{Y}_{\text{ox}} - (\mathbf{Y}_{\text{ox}} - \mathbf{Y}_{\text{fu}}) \cdot \xi \tag{2}$$

where the subscript "fu" and "ox" denote the fuel stream and the oxidizer stream, respectively.

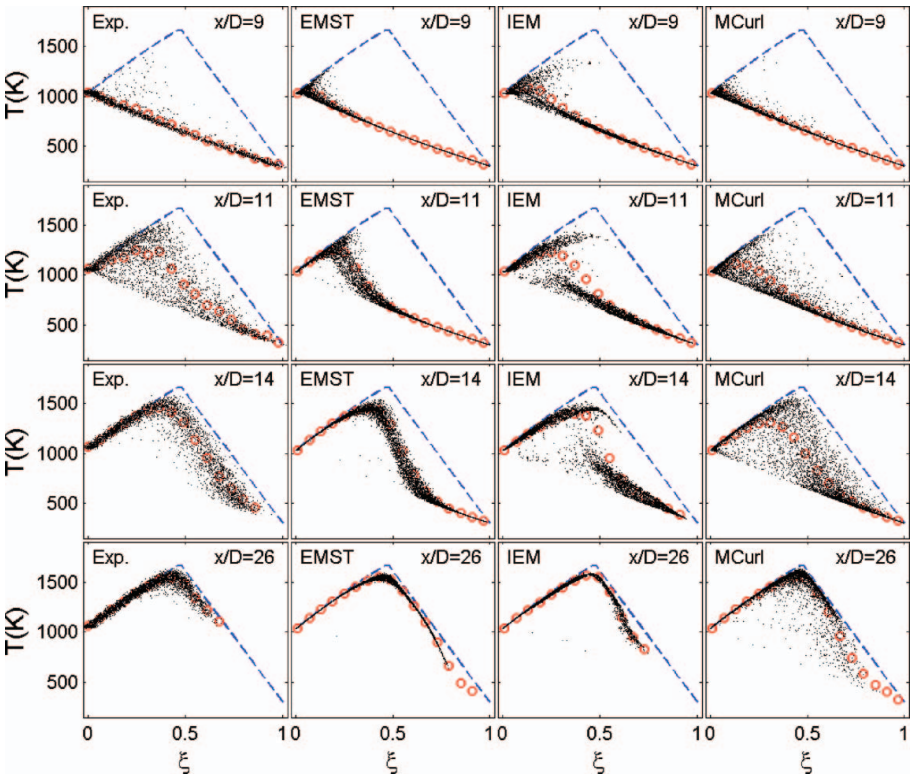

Figure 2. Scatter plots of particle temperature against mixture fraction at the axial locations x/D =9, 11, 14, and 26 in the Cabra H_2/N_2 lifted flame from experimental data and from PDF calculations using three different mixing models (Open circles: conditional mean temperature; Dashed lines: equilibrium state.)

From the experimental data at $x/D = 9$ shown in Figure 2, it may be seen that the particles lie dominantly on the mixing line, with just a few rare particles with higher temperature. This combustion stage ($x/D \leqslant 9$) is called pure mixing. For $x/D \geqslant 11$, the particles leave the mixing line gradually, indicating an ignition process. By $x/D = 26$, almost all the particles have reached the fully burnt state, close to the equilibrium line. The PDF calculations using the three mixing models predict the mixing-ignition processes reasonably well. However, the scatter plots of temperature are different for the different mixing models. Similar questions arise, e.g., how do the different mixing models cause the particles to evolve through the mixing stage to the burning state? The Eulerian data cannot answer such questions.

3. Lagrangian particle tracking

The limitations of the Eulerian data from PDF calculations are evident. In this section, we discuss the extraction of Lagrangian time series from the PDF calculations, and these are analyzed for the Sandia flame E and the Cabra lifted flame in the following two sections.

In the Lagrangian PDF method [2], the modeled transport equation for the joint PDF of the velocity $\mathbf{U}$, turbulence frequency ω, and the compositions ϕ is solved by a Monte Carlo particle method. A large number of Monte Carlo particles are released into the computational domain according to the Eulerian PDF initially. Each particle carries a full set of the fluid properties, i.e.,

$\mathbf{U}^*$, ω^*, mass m^*, locations $\mathbf{x}^*$ and ϕ^* etc. The evolution of the joint PDF is represented by the movement of the particles in the multi-dimensional space governed by the following stochastic differential equations [1–3]

$$dx_i^* = U_i^* dt, \tag{3}$$

$$dU_i^* = -\frac{1}{\langle\rho\rangle}\frac{\partial\langle p\rangle}{\partial x_i}dt - \left(\frac{1}{2}+\frac{3}{4}C_0\right)\Omega(U_i^* - \widetilde{U}_i)dt + (C_0\widetilde{k}\Omega)^{1/2}dW_i, \tag{4}$$

$$d\omega^* = -C_{\omega 3}\Omega\,(\omega^* - \widetilde{\omega})\,dt - S_\omega\Omega\omega^* dt + (2C_{\omega 3}C_{\omega 4}\tilde{\omega}\Omega\omega^*)^{1/2}\,dW, \tag{5}$$

$$\frac{d\phi_\alpha^*}{dt} = \mathcal{M}_\alpha(t) + S_\alpha\,(\phi^*(t))\,, \tag{6}$$

where ρ and p are the fluid density and pressure, respectively; "$\langle\,\rangle$" denotes the conventional mean; "$\widetilde{\ }$" denotes the Favre mean; C_0, $C_{\omega 3}$ and $C_{\omega 4}$ are model constants; $\mathbf{W}$ is an isotropic vector-valued Wiener process; W is another independent Wiener process; $\widetilde{k}$ is the turbulent kinetic energy; S_ω and S_α are the source term for ω and the reaction source term for ϕ_α, respectively; $\mathcal{M}_\alpha(t)$ denotes the mixing model; Ω is the conditional mean turbulence frequency defined as

$$\Omega \equiv C_\Omega \frac{\langle\rho^*\omega^*|\omega^* \geqslant \widetilde{\omega}\rangle}{\langle\rho\rangle}, \tag{7}$$

where the constant C_Ω is chosen so that Ω equals $\widetilde{\omega}$ in a fully turbulent region [17].

The correspondence between the statistics of the Monte Carlo particles and those of the underlying turbulent reactive flow needs careful consideration [1, 3]. A primary aim of the modeling is for the one-point, one-time joint PDF of the particles to accurately represent the same joint PDF of the fluid in the reactive flow. On the other hand, two-point, one-time statistics are radically different: in the particle system the properties at two points are statistically independent (in the infinite particle limit), and indeed two particles may have the same location $\mathbf{x}^*$ but completely different properties. Of particular relevance in the present study, is the question of correspondence of Lagrangian statistics. The Langevin equation model for velocity (Equation 4) has been constructed to be consistent with the Lagrangian velocity autocorrelation. However, the mixing models have been developed based solely on one-time Eulerian statistics, and the extent to which they represent Lagrangian statistics has not been evaluated even in simple non-reactive flows.

The solution procedure for the above equations is implemented in the code HYB2D which implements the consistent FV/particle algorithm [34]. The HYB2D code has been fully tested and validated in various papers, e.g. [23, 31, 34, 35]. This work slightly extends the HYB2D code to output the Lagrangian data.

A non-uniform mesh is used for both the FV solver and the particle tracking. The quantities at the mesh level are interpolated onto particles as needed.The statistics of particle properties on the mesh are formed from particles associated with the cell. The mixing between particles is performed within each grid cell.

The flames we are interested in are statistically stationary. The solution procedure implemented in HYB2D is a pseudo-time marching procedure. (A local time-stepping algorithm [43] is used for the marching procedure.) Starting from a "reasonable" initial condition, we march in time steps until a statistically stationary state is achieved. We continue the calculation for further time steps in order to output quantities of interest. At any time after the statistically stationary state

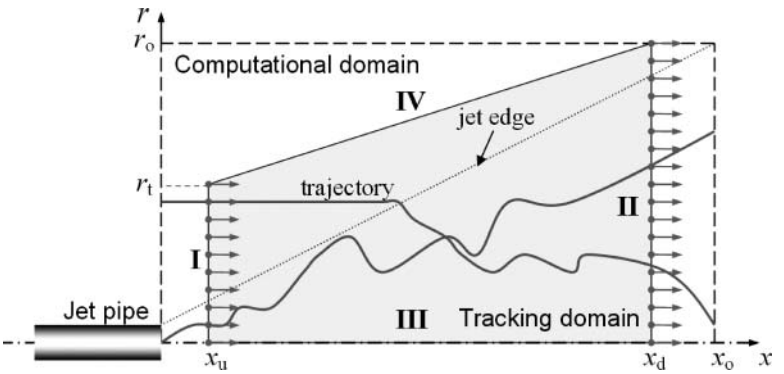

Figure 3. The computational domain and the tracking domain (consisting of four sides: **I**, **II**, **III**, and **IV**) for the jet flames.

is reached, the joint PDF is represented by a set of particles which (to some extent) model fluid particles.

Conventionally, in the PDF calculations only Eulerian data are output for postprocessing, i.e., the data at a particular time step after the statistically stationary state has been reached. Due to the Lagrangian nature of the numerical method, it is a simple matter to explore the Lagrangian data by simply exporting the particle data for many time steps after the stationary state has been reached, so that the Lagrangian particle trajectories can be formed.

Once the statistically stationary state is reached, we track a representative number N_t of particles through the active part of the flame defined as the tracking domain as shown in Figure 3. The geometry of the computational domain and the tracking domain, and the values of N_t are shown in Table 2 for the Sandia flame E and the Cabra lifted H_2/N_2 jet flame.

In the particle method, there is a particle cloning and clustering algorithm designed to maintain an approximately uniform number of particles per cell. This algorithm creates some complications for particle tracking. When a tracked particle is cloned, it splits into two or more (initially) identical particles of less weight. We arbitrarily select just one of the clones to continue the particle trajectory. When several light particles are clustered to form one heavier particle, the initial identities are lost. To prevent this problem, we suppress clustering of tracked particles (at a small cost in computational accuracy and efficiency).

Examination of the particle trajectories in physical space revealed some problems with the velocity-frequency model and its numerical implementation. These are discussed in the Appendix where a method of alleviating the problem is described.

Table 2. Geometry of the computational domain and the tracking domain, and the number of tracked particles N_t for the Sandia flame E and the Cabra lifted H_2/N_2 jet flame. See Figure 3 for definition of locations.

	x_u/D	x_d/D	x_o/D	r_t/D	r_o/D	N_t
Sandia flame E	3.0	45	80	10	20	2000
Cabra lifted flame	3.0	30	50	10	15	2000

4. Particle trajectories in Sandia flame E

PDF calculations of the Sandia flame E are performed by using the three mixing models, EMST, IEM and modified Curl. The Lagrangian tracking of particles is conducted to investigate the roles of reaction and mixing in the regions of local extinction and re-ignition. We focus on the particle behavior based on the evolution of the particle temperature in the mixture fraction space. As in the scatter plots of particles in Figures 1 and 2, and similar to the DNS analysis in [8], we divide the particle trajectories into two groups: continuous burning and local extinction. For continuous burning, the whole particle trajectory remains within the burning region (i.e., above the "extinction line"). For local extinction, some segment of the particle trajectory lies in the extinction region (below the "extinction line"). Physically, continuous burning corresponds to a stretched and distorted yet still continuous non-premixed laminar flame front, and the local extinction produces holes in the flame front [44, 45]. It should be appreciated, however, that in PDF methods there is no representation of the instantaneous flame structure. For ease of analysis, in each group, we further sub-divide the particles into different categories based upon their mixture fraction at the trajectory's initial position x_u (see Figure 3 and Table 2 for details), i.e., fuel region ($\xi < 0.1$), oxidizer region ($\xi > 0.9$), pilot stream region ($0.22 < \xi < 0.55$), and the intermediate region (all other values of ξ).

In the flames considered here, the particle axial distance $x^*(t)$ is an increasing function of time t. To some extent, the axial distance can be viewed as a time-like variable since the particles do not flow backwards in the axial direction. Since we are more interested in local extinction and re-ignition at different axial locations, it is more revealing to explore the particle time series with respect to the axial distance x/D rather than with respect to time.

4.1. *Trajectories of continuously burning particles*

The trajectories of continuously burning particles from the fuel region in flame E are shown in Figures 4–6 for PDF calculations using the different mixing models. Only 25 particles randomly chosen from the tracking dataset are shown for each category. The circles in the plots show the current compositions of particles, and the lines connect their past compositions. For each figure of particle trajectories (such as Figures 4–6), the supplementary material includes a corresponding animation. These animations show the evolution with axial distance of all tracked particles' compositions. In the temperature-mixture fraction 2-D plane in Figures 4–6, chemistry can only change the particle positions vertically due to element conservation during reaction (conservation of mixture fraction ξ), while mixing can move the particles both vertically and horizontally.

The general observations on the trajectories of the continuously burning particles calculated using the different mixing models are the following. First, the mixture fraction of particles can vary in the whole mixture fraction range, e.g., initially ξ^* is greater than 0.9 for all particles, while later ξ^* is less than 0.1 for some particles in Figures 4–6. As discussed before, this change is solely caused by mixing, indicating the important role of mixing in turbulent combustion. Second, different particles have completely different trajectories as expected in a turbulent flow. Third, at different stages of the particle evolution, the roles of reaction and mixing are different. In Figures 4–6, the particles from the fuel region tend to come close to the extinction line when first approaching the stoichiometric condition ($\xi = 0.351$). At around the stoichiometric condition in Figures 4–6, we can observe that some particles suddenly shoot upward (e.g., at x/D=18, some particle trajectories become nearly vertical). Apparently, in this stage, the reaction time scale is much less than the mixing time scale, and reaction becomes dominant. A quantitative presentation of the relative roles of mixing and reaction is discussed in Section 6.

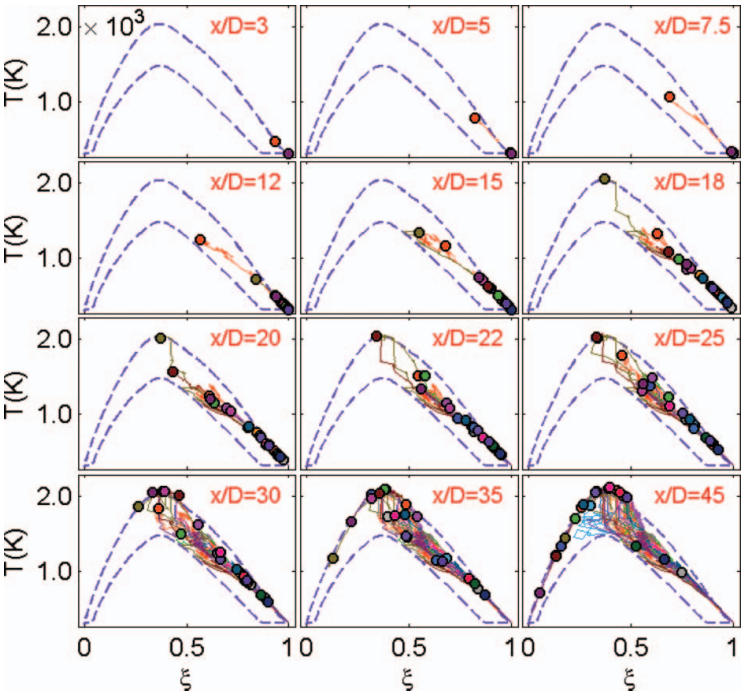

Figure 4. The continuous burning particle trajectories from the fuel region in flame E by the EMST model. (This [link] provides an animation of these particle trajectories.)

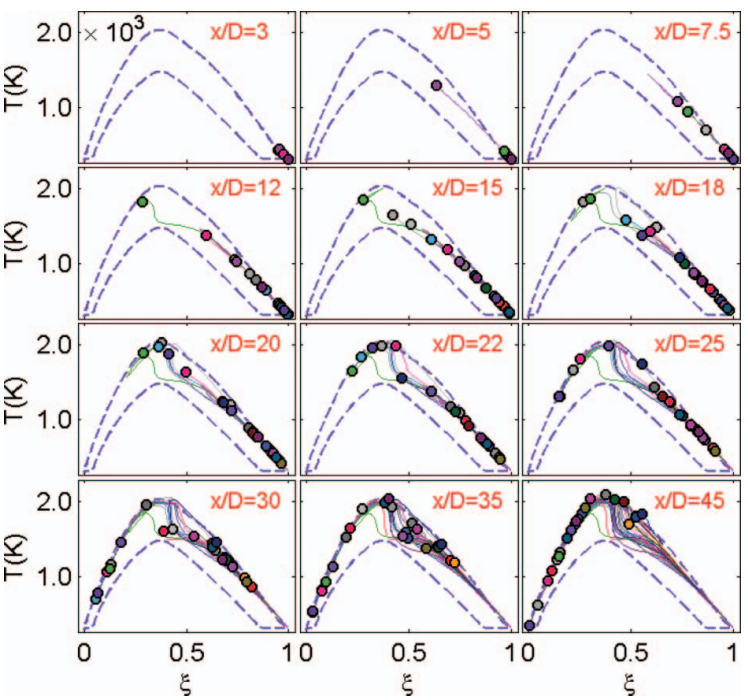

Figure 5. The continuous burning particle trajectories from the fuel region in flame E by the IEM model. (This [link] provides an animation of these particle trajectories.)

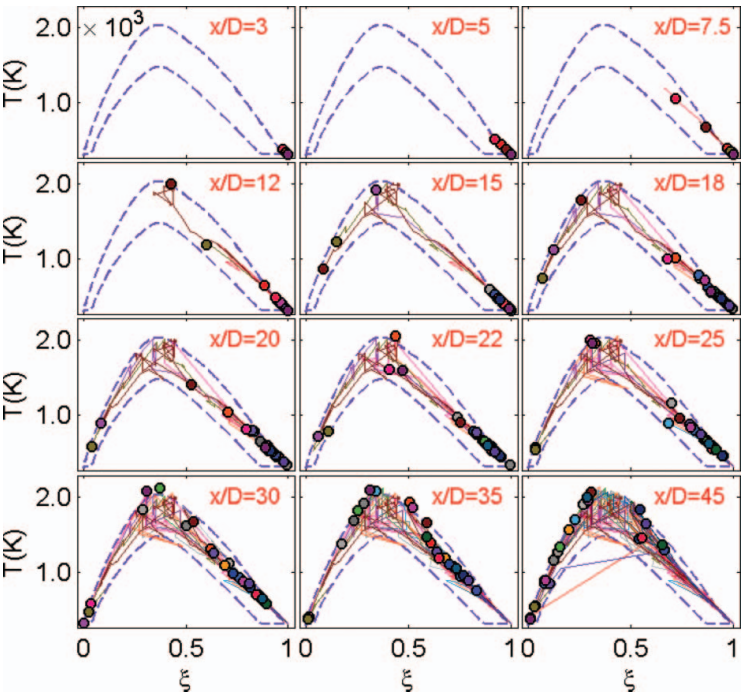

Figure 6. The continuous burning particle trajectories from the fuel region in flame E by the modified Curl model. (This [link] provides an animation of these particle trajectories.)

The particle behavior simulated by the different mixing models is qualitatively different. The particle trajectories produced by the EMST model are continuous but non-differentiable [21]. These trajectories are not smooth in Figure 4. The trajectories by the IEM model are continuous and differentiable, and the simulated trajectories are smooth and are clear in Figure 5. It is easy to follow each particle from the plot, making the observation and analysis much easier. The trajectories arising from the modified Curl model are discontinuous. The particles jump in composition space, possibly resulting in the direct mixing of a cold fuel particle and a cold oxidizer particle. This can be observed at $x/D = 45$ in Figure 6. Two particles with very lean and very rich mixtures are connected, indicating the jumping of the particle from the one side to the other side instantaneously. (For continuously burning particles, by definition, their compositions at no time lie in the extinction region, which means the straight lines across the extinction region at $x/D = 45$ in Figure 6 correspond to an instantaneous jump in particle composition.) This jump behavior by the modified Curl makes the particle trajectories difficult to follow.

Similar observations can be made from the trajectories of continuously burning particles from other categories (oxidizer region, pilot stream region and the intermediate region). Due to space limitations, these trajectories are not shown here.

4.2. *Trajectories of locally extinguished particles*

4.2.1. *Particle trajectories from the EMST model*

The locally extinguished particle trajectories originating from different regions in calculations using the EMST mixing model are shown in Figures 7–9.

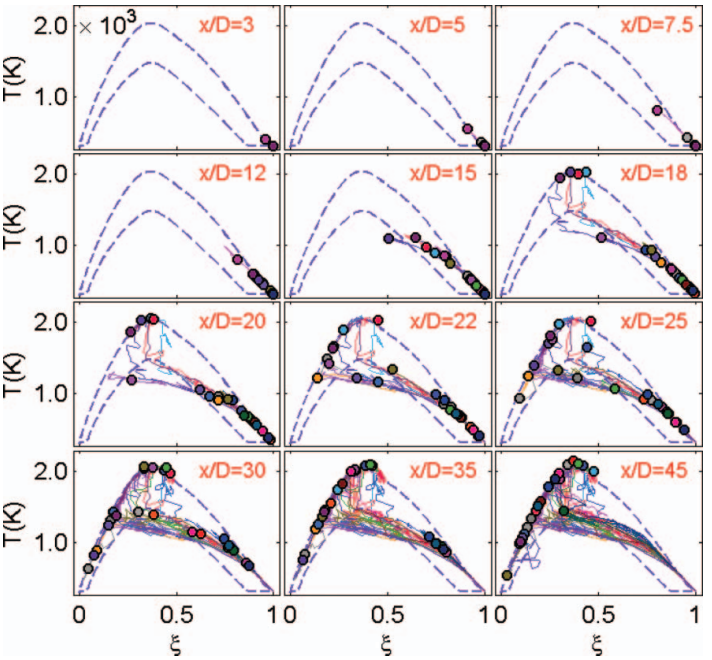

Figure 7. Trajectories of locally extinguished particles from the fuel region in flame E by the EMST model. (This [link] provides an animation of these particle trajectories.)

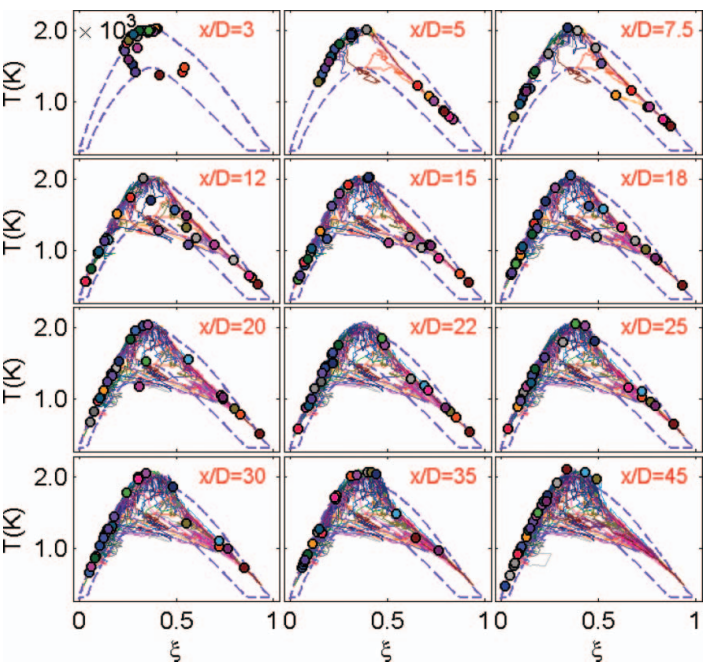

Figure 8. Trajectories of locally extinguished particles from the pilot stream region in flame E by the EMST model. (This [link] provides an animation of these particle trajectories.)

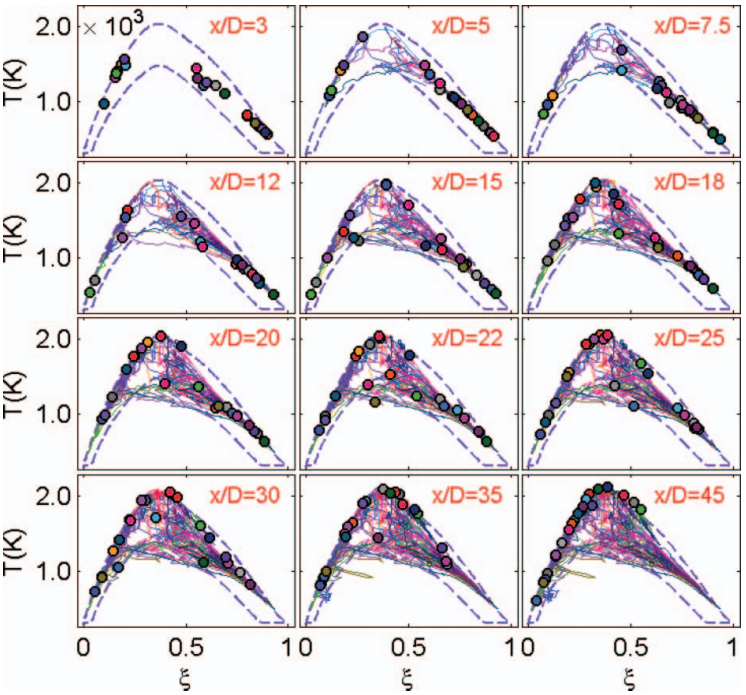

Figure 9. Trajectories of locally extinguished particles from the intermediate region in flame E by the EMST model. (This [link] provides an animation of these particle trajectories.)

Figure 7 shows the trajectories of particles initially from the fuel region. In the temperature-mixture fraction space, the mixture fraction of particles first decreases, and the particles come close to the extinction line. Around $\xi = 0.6$, the particles enter the extinction region, and become locally extinguished according to our criterion for extinction. The particle trajectories inside the extinction region become nearly horizontal (little temperature rise), implying that mixing is at least as rapid as reaction. The return of the particles to the burning region corresponds to re-ignition. From Figure 7, two different re-ignition processes can be observed. First, at around the stoichiometric condition, some trajectories of extinguished particles turn and move upward to return to the burning state, e.g., at $x/D = 18$ in Figure 7 we can observe four trajectories of extinguished particles moving dominantly upward to return to the burning state. During this re-ignition process, the mixture fraction of the particles changes slightly while the temperature rises by more than 600 K. Although re-ignition is the result of mixing and reaction, reaction seems dominant in this re-ignition process, which is similar to auto-ignition. The local extinction induced by the mixing causes the coexistence of fuel and oxidizer in the same particle, and the temperature of these particles is greater than 1000 K, e.g., one particle in the extinction region at $x/D = 15$ in Figure 7. Given appropriate conditions (e.g., induction period and a relatively long mixing time scale), the auto-ignition brings the particles back to the burning state. We refer to this re-ignition mechanism as an auto-ignition mechanism. Second, instead of auto-ignition, the other extinguished particles keep moving in the same direction (nearly horizontally to the left) and re-enter the burning state on the lean side of stoichiometric, e.g., from $x/D = 20$ to 45. During this process, mixing is at least as rapid as reaction. We call this mechanism the mixing-reaction mechanism. It is worth mentioning that the above two re-ignition mechanisms are identified in

the DNS study [11]. The particles from the oxidizer region (not shown) behave similarly to the particles from the fuel region. The two different re-ignition processes are also observed there.

Figure 8 shows the trajectories of the particles from the pilot stream region in flame E when using the EMST model. The pilot stream is used to stabilize the flame. From Figure 8, for this subset of particles (all of which enter the extinction region at some time), they dominantly enter the extinction region from the lean and rich sides, after there has been mixing essentially along the fully burnt line. Only one or two particles enter the extinction region from above around stoichiometric.

In Figure 9 are shown the trajectories of the particles from the intermediate region in flame E using the EMST model. Initially ($x/D \leqslant 7.5$) the particle composition changes due to mixing and reaction and remains, predominantly, in the burning region. The local extinction observable for $12 \leqslant x/D \leqslant 25$ occurs dominantly by mixing drawing rich and lean particles nearly horizontally into the extinction region.

In summary, the local extinction and re-ignition processes in the Sandia flame E are illustrated by tracking particles using the EMST model. Two different re-ignition mechanisms are observed in the flame by using the EMST model, i.e. auto-ignition and mixing-reaction. The investigation of the mixing models in conjunction with the large eddy simulations using the DNS data by Mitarai *et al*. [10] demonstrates the very good performance of the EMST mixing model in predicting the particle behavior in the regions of local extinction and re-ignition. The above observed particle behavior by the EMST is expected to represent the actual situation qualitatively.

4.2.2. *Particle trajectories using the IEM and modified Curl models*

The trajectories of the particles from the fuel region in flame E using the IEM model are shown in Figure 10. Following each particle trajectory, we can observe the similar local extinction and re-ignition processes as in the case of the EMST model (shown in Figure 7). The two re-ignition mechanisms can also be identified: auto-ignition and mixing-reaction. The re-ignition process for the IEM model, however, is somewhat different from that for the EMST model in Figure 7. In Figure 7, the re-igniting particles for the EMST model tend to move almost horizontally first with a slight temperature rise, and then either move upward due to the auto-ignition mechanism or keep moving horizontally due to the mixing-reaction mechanism without an obvious temperature drop before entering the burning region. In Figure 10, however, some of the re-igniting particles induced by the auto-ignition mechanism experience a temperature drop before ignition. Almost all the re-igniting particles induced by the mixing-reaction mechanism tend to decrease their temperature significantly before entering the burning region. For the IEM model at the early stages of re-ignition, this behavior is explained by the fact that the mean temperature (to which the particle temperature relaxes) is lower than that of the particles, which are about to re-ignite, since these are the hottest particles in the ensemble. To some extent this reflects the physics of the problem in that conduction cools fluid at a local temperature maximum. The trajectories of the particles from the other regions in flame E using the IEM model (not shown) show similar behavior to those from the fuel region in Figure 10.

Figure 11 shows the particle trajectories from the fuel region using the modified Curl model. The jumps in the particle properties make the understanding of particle behavior more difficult. The particle evolution is generally quite similar to the IEM model. Local extinction and re-ignition are predicted, and the two re-ignition mechanisms can be observed. However, similar to the IEM model, the re-igniting particles tend to have some temperature drop before or during the re-ignition, which is not observed in the EMST results. The trajectories of the particles from the other regions in flame E using the modified Curl model (not shown) show similar behavior to those from the fuel region in Figure 11.

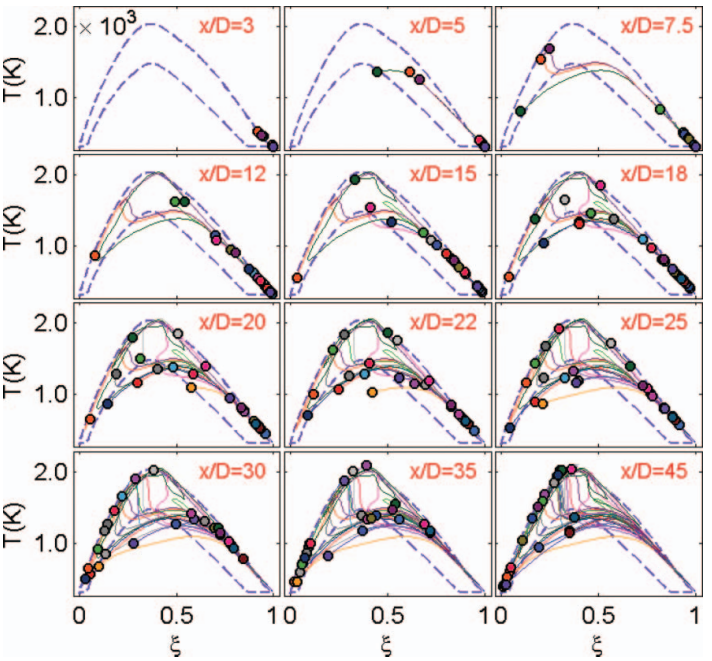

Figure 10. Trajectories of locally extinguished particles from the fuel region in flame E using the IEM model. (This [link] provides an animation of these particle trajectories.)

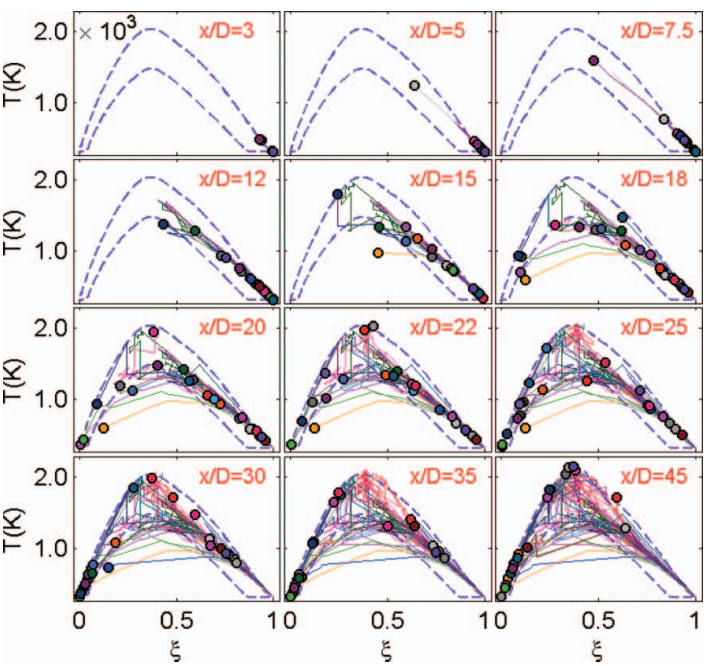

Figure 11. Trajectories of locally extinguished particles from the fuel region in flame E using the modified Curl model. (This [link] provides an animation of these particle trajectories.)

In this sub-section, the local extinction and re-ignition processes in the Sandia flame E are illustrated by tracking particles using the IEM and modified Curl models. The two re-ignition mechanisms (auto-ignition and mixing-reaction) identified by using the EMST model in Figure 7 are also observed here by using these two mixing models. However, the re-igniting particles by these two mixing models have somewhat different behavior from those by the EMST model, i.e., a temperature drop before or during the re-ignition. This difference in re-ignition by the different mixing models is not clear yet because there is no experimental data on Lagrangian trajectories in the flame. Nevertheless, the two identified re-ignition mechanisms and the different particle behavior during the re-ignition by the different mixing models cannot be observed with the Eulerian particle data, and the observations contribute to our understanding of the performance of the models.

5. Particle trajectories in Cabra H_2/N_2 lifted flame

Previous studies [31, 32] suggest that auto-ignition is a dominant mechanism in the stabilization of the Cabra H_2/N_2 lifted flame. In addition, both experimentally [33] and in modeling studies [31], it is found that the flames are extremely sensitive to the temperature of the vitiated coflow. To further understand and characterize these processes, we first perform auto-ignition tests in which the ignition delay time (IDT) is calculated as a function of mixture fraction and coflow temperature. The initial condition of the tests satisfies Equations (1)–(2). The fuel stream and the oxidizer stream in the tests are the same as those in the Cabra lifted flame. The coflow (oxidizer) temperature varies from $T_c = 1022$ K to 1080K. Figure 12 shows the IDTs of the mixture for different coflow temperatures. The IDT is defined here as the time when the mixture temperature reaches the mid-point between the initial temperature and the equilibrium temperature. The strong sensitivity of the IDTs to the coflow temperature is evident from the plot, which is consistent with the findings in [31]. The shortest IDTs occur at the very fuel-lean region, around $\xi = 0.04$. The stoichiometric condition is $\xi = 0.47$ in the flame. The IDTs varies by three orders of magnitude over the range of mixture fraction shown.

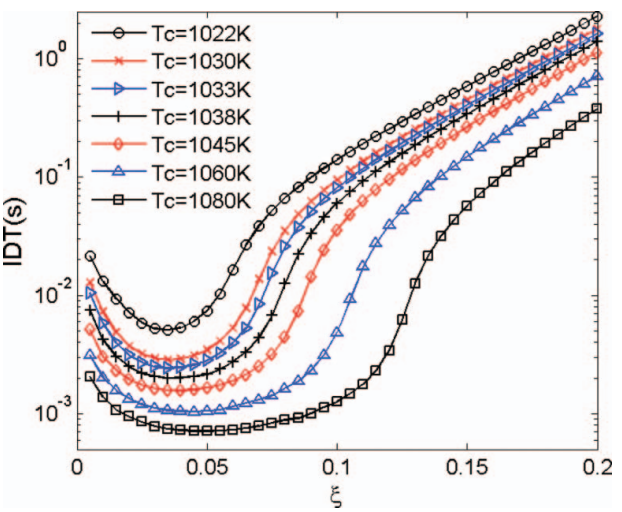

Figure 12. The ignition delay time (IDT) of $H_2/N_2/O_2$ mixture for different coflow temperature T_c.

The PDF calculations of the Cabra H_2/N_2 lifted flame are performed by using the three mixing models, EMST, IEM and modified Curl. The Lagrangian tracking of particles is conducted to investigate the roles of reaction and mixing in the flame. The tracking details are shown in Table 2. As in the analysis of flame E in Section 4, we focus on the particle behavior based on the evolution of the particle temperature in mixture fraction space. The particle trajectories are divided into different categories based upon their mixture fraction at the trajectory initial position x_u, i.e., fuel region ($\xi < 0.1$), oxidizer region ($\xi > 0.9$), and the intermediate region between the fuel and the oxidizer region. For each category, 100 particles randomly chosen from the tracking dataset are shown in the following figures, whereas all tracked particles are shown in the corresponding animations in the supplementary material.

Figure 13 shows the trajectories of the particles from the fuel region in the Cabra lifted flame using the EMST model. Initially, ($x/D \leqslant 9$) the particles move in the plane exclusively by mixing. A particle trajectory due to pure mixing is a nearly straight line between the cold fuel temperature and the hot coflow temperature. Pure mixing yields a partially premixed mixture of fuel and oxidizer at different mixture fractions. At about $x/D = 10$, some particles near the oxidizer side start to ignite first due to their short IDTs as shown in Figure 12. The ignition mechanism of the first few particles is expected to be auto-ignition, similar to the auto-ignition of the homogeneous mixture in Figure 12.

After the rapid auto-ignition of the first few particles, these relatively hot burnt particles at $x/D > 11$ in Figure 13 mix with adjacent particles in composition space, thus raising their temperature (and radical concentration) and hence promoting their auto-ignition. Therefore the ignition progressively moves to richer mixtures. This burning process is not exclusively the auto-ignition of the particles. Both reaction and mixing play important roles. A plausible physical picture of the processes involved in the Cabra flame is that some regions under the fuel-lean condition ignite first after the induction period given an appropriate mixing condition. These ignition spots are distributed in the physical space separately. After the high temperature ignition spots are formed, they propagate toward each other and merge into a connected premixed flame front. This picture is supported by the DNS study of the auto-ignition of mixing layers between cold fuel and hot oxidizer in an isotropic and homogeneous turbulence flow [46]. The evolution of the particles using EMST in Figure 13 is consistent with this picture, even though the spatial structure of the instantaneous flame is not explicitly represented. We simply name this ignition process as mixing-ignition. By $x/D = 30$ in Figure 13, all the particles shown reach the full burnt state close to the equilibrium line. From the particle trajectories in the Cabra lifted jet flame using the EMST model, we can observe the whole mixing-reaction process. Four stages of combustion can be identified, i.e. pure mixing, auto-ignition, mixing-ignition, and fully burnt. Apparently, this combustion detail cannot be observed from the Eulerian data like the scatter plot in Figure 2. The particles from the other regions in the Cabra lifted flame by using EMST model (not shown) show the similar ignition dynamics.

In Figure 14 are shown the trajectories of the particles from the fuel region in the Cabra lifted flame using the IEM model. Pure mixing occurs for $x/D < 10$. At the locations between $x/D = 10$ and 11, a few particles near the oxidizer side (brought there by mixing) start to auto-ignite. After the auto-ignition of the first few particles, the temperature of other particles in the rich region is raised through their mixing with the elevated mean, and the ignition of these particles is promoted. Mixing and reaction play important roles in this ignition process. As in the EMST model, this ignition process can be named as mixing-ignition. The particle behavior in this ignition process for the IEM model is slightly different from that for the EMST model in Figure 13. The EMST model is local in composition space. Hence the burnt particles at given ξ^* mix with particles around the same value of ξ^*. While in the IEM model all particles mix towards the mean. In spite of the different particle behavior, four stages of combustion can be identified

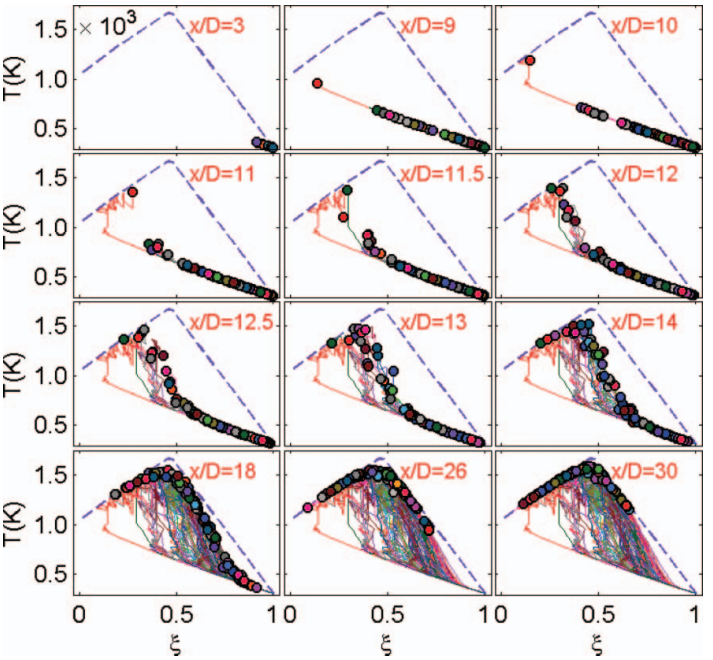

Figure 13. Particle trajectories from the fuel region in the Cabra lifted flame using the EMST model. (This [link] provides an animation of these particle trajectories.)

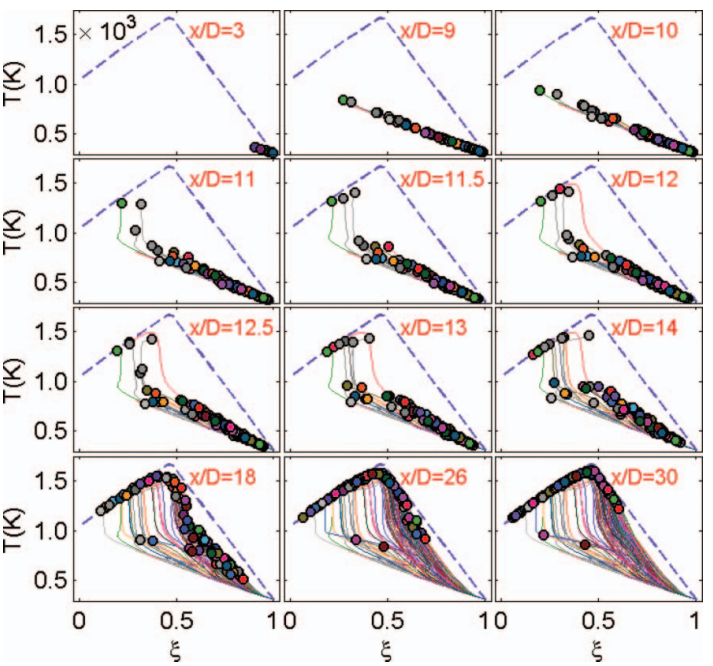

Figure 14. Particle trajectories from the fuel region in the Cabra lifted flame using the IEM model. (This [link] provides an animation of these particle trajectories.)

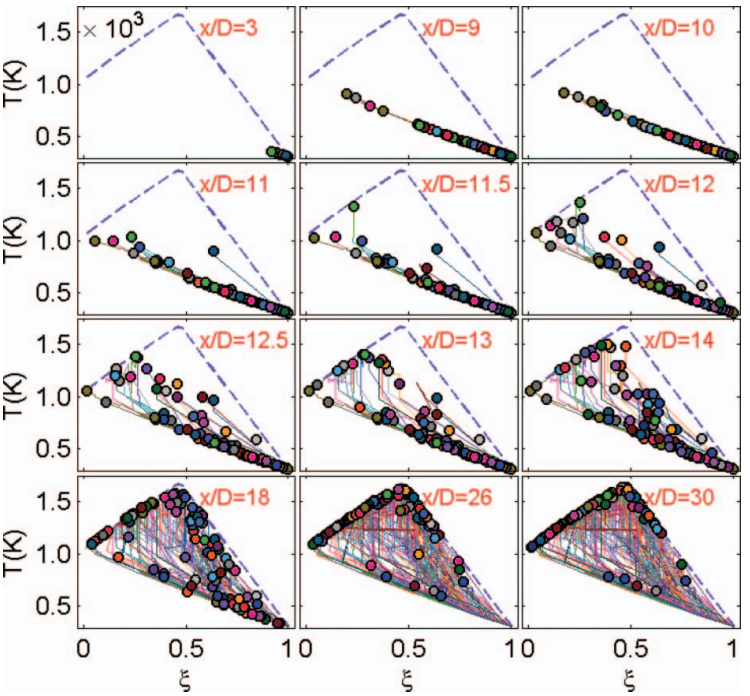

Figure 15. The particle trajectories from the fuel region in the Cabra lifted flame by the modified Curl model. (This [link] provides an animation of these particle trajectories.)

for the IEM as those in the EMST model. The trajectories of the particles from the other regions (not shown) show similar particle behavior for IEM model as in Figure 14.

In Figure 15 are shown the particle trajectories from the fuel region in the Cabra lifted flame using the modified Curl model. The modified Curl model can reproduce the same four combustion stages in the flame identified by the previous two mixing models. As in the IEM model, the particle behavior in the mixing-ignition stage by the modified Curl model is also different from that by the EMST model due to the non-localness of the model in the composition space. The particle trajectories from the other regions in the Cabra lifted flame using the modified Curl model (not shown) show the same behavior.

In this section, the particle trajectories using the different mixing models are investigated in the Cabra H_2/N_2 lifted flame. The particle behavior by the IEM and modified Curl models is different from that by the EMST model, because of the non-localness of the IEM and modified Curl models compared to the localness property of the EMST model. In spite of the different individual particle behavior, the overall combustion processes revealed by the different mixing models are similar, and four stages of combustion in the flame can be identified, i.e. pure mixing, auto-ignition, mixing-ignition, and fully burnt. In some sense, this finding is consistent with the DNS study of an auto-ignition problem in homogeneous isotropic turbulence [46], even though the particles do not provide a direct representation of spatial structure. This contributes to our understanding of the model performance in the turbulent lifted jet flames.

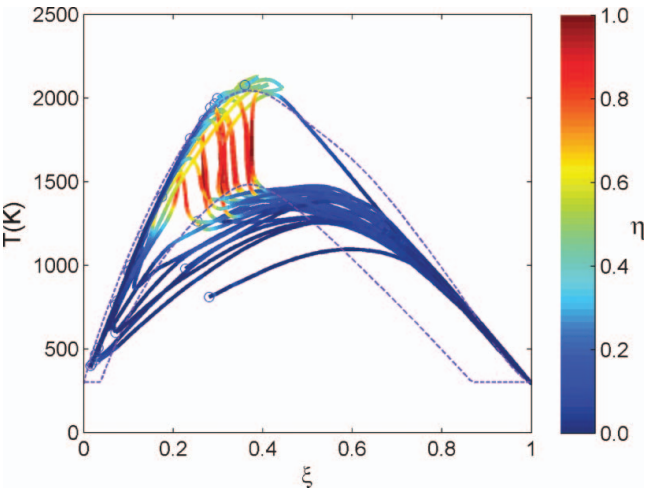

Figure 16. Trajectories (up to $x/D = 45$) color-coded by parameter η (Equation 10) of locally extinguished particles from the fuel region in flame E using the IEM model.

6. Roles of mixing and reaction during re-ignition and auto-ignition

In the previous sections, the roles of mixing and reaction during the particle evolution are discussed qualitatively. The relative importance of mixing and reaction for each particle as it evolves can be quantified by examining the mixing rate given by the mixing models relative to the reaction rate. For this purpose we define the mixing rate $\dot{\mathcal{M}}$ and reaction rate $\dot{S}$ for each particle as,

$$\dot{\mathcal{M}} = \sqrt{\left(\frac{d\xi}{dt}\right)^2 + \left(\frac{1}{T_{ref}}\frac{dT}{dt}\right)^2}\Bigg|_{\text{mix}}, \tag{8}$$

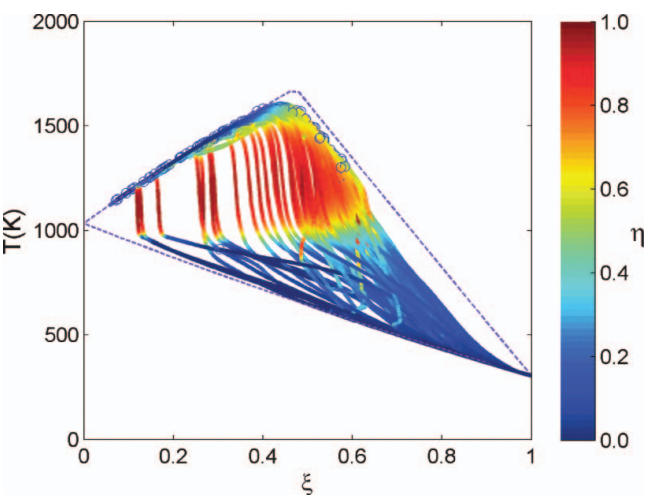

Figure 17. Particle trajectories (up to $x/D = 30$) color-coded by parameter η (Equation 10) from the fuel region in the Cabra lifted flame using the IEM model

and

$$\dot{S} = \left| \frac{1}{T_{ref}} \frac{dT}{dt} \right|_{\text{react}}, \tag{9}$$

where $T_{ref} = 2000$ K, and in Equations (8) and (9) the rates of change pertain solely to the effects of mixing and reaction, respectively. (In the computations, these quantities are readily evaluated based on the particle properties before and after the mixing and reaction fractional steps.)

The relative importance of mixing and reaction can be quantified by the parameter

$$\eta = \frac{S}{S + \mathcal{M}}, \tag{10}$$

which varies between zero (corresponding to no reaction) and one (corresponding to no mixing).

We focus our investigation on the IEM mixing model. For the modified Curl model, the composition changes discontinuously, and so $d\xi/dt|_{\text{mix}}$ is not well defined. For the EMST mixing model, $d\xi/dt|_{\text{mix}}$ exhibits large fluctuations of small time scale which obscure the picture.

Figure 16 shows, for flame E, trajectories color-coded by the parameter η of locally extinguished particles initially from the fuel region. From the figure, we can clearly see the relative importance of mixing and reaction during re-ignition. For the particles re-igniting due to auto-ignition mechanism, the reaction is dominant ($\eta \approx 1.0$) when the particles shoot upward at around stoichiometric condition. For those particles which re-ignite due to mixing-reaction, either both mixing and reaction are important (e.g., $\eta \approx 0.3$ for one particle entering the burning region at about $T = 1100$K), or mixing is dominant due to the low temperature.

In Figure 17, the particle trajectories originating from fuel stream in the Cabra flame are shown. In the current simulation of the Cabra flame, the initial ignition process occurs when particles leave the pure mixing line between cold fuel and hot coflow. From the figure, it may be seen that the particle starting to ignite at fuel-lean side leave the pure mixing line dominantly by reaction, corresponding to the auto-ignition identified before. The particles leaving the pure mixing line on the fuel-rich side experience two stages: a mixing-dominant stage to raise the particle temperature to about 1000K, and reaction-dominant stage to raise the particle temperature close to the equilibrium. Both mixing and reaction are important for the ignition of these particles, and they correspond to the previously identified mixing-ignition process. The particle trajectories along with the rates of mixing and reaction provide insights on the roles of mixing and reaction during re-ignition and auto-ignition.

7. Conclusion

Lagrangian PDF investigations of the Sandia piloted flame E and the Cabra H_2/N_2 lifted flame are performed to help obtain a deeper understanding of the modeling of local extinction, re-ignition and auto-ignition in these flames. Eulerian scatter plots (shown in Figures 1–2) of the two flames from the PDF calculations are reviewed to show the limitations of one-time statistics. A Lagrangian particle tracking procedure is implemented in the code HYB2D. Lagrangian particle data are extracted from the PDF calculations after the statistically stationary state is reached, in order to explore the PDF result more comprehensively.

Lagrangian particle tracking in the PDF calculations of Sandia flame E is performed for the different mixing models, EMST, IEM and modified Curl. The particle trajectories are divided into two groups, continuous burning and local extinction. For each group, the trajectories are further sub-divided into different categories based on the original particle locations: the fuel steam, the

oxidizer stream, the pilot stream, and the intermediate region. The particle trajectories given by the different mixing models are different, i.e., continuous but non-differentiable by EMST, continuous and differentiable by IEM, and discontinuous by modified Curl. All three mixing models reproduce the local extinction and re-ignition processes reasonably. Two different re-ignition mechanisms are identified, the auto-ignition mechanism and the mixing-reaction mechanism.

Homogeneous auto-ignition tests for the same condition as in the Cabra H_2/N_2 lifted flame are conducted. The lowest ignition delay time (IDT) occurs at a very fuel-lean condition for a range of coflow (oxidizer) temperatures. The strong sensitivity of the IDTs to the coflow temperature is observed, which is also reported in previous PDF calculations of the Cabra lifted flame [31].

Lagrangian particle tracking in the PDF calculations of the Cabra H_2/N_2 lifted is also performed for the different mixing models. The particle trajectories are divided into different categories based on the original particle locations: the fuel stream, the oxidizer stream, and the intermediate region. The models reproduce the whole auto-ignition process reasonably. Four stages of combustion in the Cabra flame are identified in the calculations, i.e., pure mixing, auto-ignition, mixing-ignition, and fully burnt.

The roles of mixing and reaction during re-ignition and auto-ignition are investigated by using IEM. The relative importance of mixing and reaction is quantified for particles during re-ignition and auto-ignition.

Acknowledgements

This work is supported by the Air Force Office of Scientific Research, Grant FA9550-06-1-0048 and by Department of Energy, Grant DE-FG02-90ER. Various suggestions from David A. Caughey, Zhuyin Ren and Steven R. Lantz are appreciated. This research was conducted using the resources of the Cornell Theory Center, which receives funding from Cornell University, New York State, federal agencies, foundations, and corporate partners.

References

[1] Pope, S.B., 1985, PDF methods for turbulent reactive flows. *Progress in Energy and Combustion Science,* **11**, 119–192.
[2] Pope, S.B., 1994, Stochastic Lagrangian models for turbulence. *Annual Reviews of Fluid Mechanics,* **26**, 23–63.
[3] Pope, S.B., 2000, *Turbulent Flows* (Cambridge University Press, Cambridge, UK).
[4] Xu, J., Pope, S.B., 2000, PDF calculations of turbulent nonpremixed flames with local extinction. *Combustion and Flame,* **123**, 281–307.
[5] Lindstedt, R.P., Louloudi, S.A., Vaos, E.M., 2000, Joint scalar probability density function modeling of pollutant formation in piloted turbulent jet diffusion flames with comprehensive chemistry. *Proceedings of the Combustion Institute,* **28**, 149–156.
[6] Yeung, P.K., 2001, Lagrangian characteristics of turbulence and scalar transport in direct numerical simulations. *Journal of Fluid Mechanics,* **427**, 241–274.
[7] Yeung, P.K., 2002, Lagrangian investigations of turbulence. *Annual Reviews of Fluid Mechanics,* **34**, 115–142.
[8] Mitarai, S., Riley, J.J., Kosaly, G., 2003, A Lagrangian study of scalar diffusion in isotropic turbulence with chemical reaction. *Physics of Fluids,* **15**, 3856–3866.
[9] Mitarai, S., Kosaly, G., Riley, J.J., 2004, A new Lagrangian flamelet model for local flame extinction and reignition. *Combustion and Flame,* **137**, 306–319.
[10] Mitarai, S., Riley, J.J., Kosaly, G., 2005, Testing of mixing models for Monte Carlo probability density function simulations. *Physics of Fluids,* **17**, 047101.
[11] Sripakagorn, P., Mitarai, S., Kosaly, G., Pitsch, H., 2004, Extinction and reignition in a diffusion flame: a direct numerical simulation study. *Journal of Fluid Mechanics,* **518**, 231–259.

[12] Voth, G.A., Satyanarayan, K., Bodenschatz, E., 1998, Lagrangian acceleration measurements at large Reynolds numbers. *Physics of Fluids,* **10**, 2268–2280.
[13] La Porta, A., Voth, G.A., Crawford, A.M., Alexander, J., Bodenschatz, E., 2001, Fluid particle accelerations in fully developed turbulence. *Nature,* **409**, 1017–1019.
[14] Mordant, N., Leveque, E., Pinton, J.-F., 2004, Experimental and numerical study of the Lagrangian dynamics of high Reynolds turbulence. *New Journal of Physics,* **6**, 116–159.
[15] Barlow, R.S., Frank, J.H., 1998, Effects of turbulence on species mass fractions in methane-air jet flames. *Proceedings of the Combustion Institute,* **27**, 1087–1095.
[16] Cabra, R., Myhrvold, T., Chen, J.-Y., Dibble, R.W., Karpetis, A.N., Barlow, R.W., 2002, Simultaneous laser Raman-Rayleigh-Lif measurements and numerical modeling results of a lifted turbulent H-2/N-2 jet flame in a vitiated coflow. *Proceedings of the Combustion Institute,* **29**, 1881–1888.
[17] Van Slooten, P.R., Jayesh, Pope, S.B., 1998, Advances in PDF modeling for inhomogeneous turbulent flows. *Physics of Fluids,* **10**, 246–265.
[18] Villermaux, J., Devillon, J.C., 1972, Représentation de la coalescence et de la redispersion des domaines de ségrégation dans un fluide per modéle d'interaction phénoménoloqique. In: *Proceedings of the Second International Symposia on Chemical Reaction Engineering*, Elsevier, New York.
[19] Dopazo, C., O'Brien, E.E., 1974, An approach to the autoignition of a turbulent mixture. *Acta Astronautica,* **1**, 1239–1266.
[20] Janicka, J., Kolbe, W., Kollmann, W., 1979, Closure of the transport-equation for the probability density function of turbulent scalar fields. *Journal of Non-Equilibrium Thermodynamics,* **4**, 47–66.
[21] Subramaniam, S., Pope, S.B., 1998, A mixing model for turbulent reactive flows based on Euclidean minimum spanning trees. *Combustion and Flame,* **115**, 487–514.
[22] Nooren, P.A., Wouters, H.A., Peeters, T.W.J., Roekaerts, D., Maas, U., Schmidt, D., 1997, Monte Carlo PDF modelling of a turbulent natural-gas diffusion flame. *Combustion Theory and Modelling,* **1**, 79–96.
[23] Cao, R.R., Wang, H., Pope, S.B., 2007, The effect of mixing models in PDF calculations of piloted jet flames. *Proceedings of the Combustion Institute,* **31**, 1543–1550.
[24] Ren, Z., Subramaniam, S., Pope, S.B., 2004, Implementation of the EMST mixing model, http://eccentric.mae.cornell.edu/∼tcg/emst.
[25] Klimenko, A.Y., Pope, S.B., 2003, A model for turbulent reactive flows based on multiple mapping conditioning. *Physics of Fluids,* **15**, 1907–1925.
[26] Pope, S.B., 1994, On the relationship between stochastic Lagrangian models of turbulence and second-moment closures. *Physics of Fluids,* **6**, 973–985.
[27] Fox, R.O., 1996, On velocity conditioned scalar mixing in homogeneous turbulence. *Physics of Fluids,* **8**, 2678–2691.
[28] Pope, S.B., 1998, The vanishing effect of molecular diffusivity on turbulent dispersion: implications for turbulent mixing and the scalar flux. *Journal of Fluid Mechanics,* **359**, 299–312.
[29] Sawford, B.L., 2004, Micro-Mixing Modelling of Scalar Fluctuations for Plumes in Homogeneous Turbulence. *Flow, Turbulence and Combustion,* **72**, 133–160.
[30] Cao, R.R., Pope, S.B., 2005, The influence of chemical mechanisms on PDF calculations of non-premixed piloted jet flames. *Combustion and Flame,* **143**, 450–470.
[31] Cao, R.R., Pope, S.B., Masri, A.R., 2005, Turbulent lifted flames in a vitiated coflow investigated using joint PDF calculations. *Combustion and Flame,* **142**, 438–453.
[32] Masri, A.R., Cao, R., Pope, S.B., Goldin, G.M., 2004, PDF Calculations of Turbulent Lifted Flames of H2/N2 issuing into a vitiated co-flow. *Combustion Theory and Modelling,* **8**, 1–22.
[33] Wu, Z., Starner, S.H., Bilger, R.W., 2005, Lift-off heights of turbulent H2/N2 jet flames in a vitiated co-flow. in: D.R. Honnery (Ed.), *Proceedings of the 2003 Australian Symposium on Combustion and the Eighth Australian Flame Days,* The Combustion Institute.
[34] Muradoglu, M., Pope, S.B., Caughey, D.A., 2001, The hybrid method for the PDF equations of turbulent reactive flows: consistency conditions and correction algorithms. *Journal of Computational Physics,* **172**, 841–878.
[35] Wang, H., Pope, S.B., 2008, Time averaging strategies in the finite-volume/particle hybrid algorithm for the joint PDF equation of turbulent reactive flows. *Combustion Theory and Modelling* (DOI: 10.1080/13647830701847875).
[36] Pope, S.B., 1997, Computationally efficient implementation of combustion chemistry using in situ adaptive tabulation. *Combustion Theory and Modelling,* **1**, 41–63.

[37] Smith, G.P., Golden, D.M., Frenklach, M., Moriarty, N.W., Eiteneer, B., Goldenberg, M., Bowman, C.T., Hanson, R.K., Song, S., Gardiner Jr., W.C., Lissianski, V.V., Qin, Z., http://www.me.berkeley.edu/gri_mech/.
[38] Li, J., Zhao, Z., Kazakov, A., Dryer, F.L., 2003, An updated comprehensive kinetic model for H_2 combustion. in: *Fall Technical Meeting of the Eastern States Section of the Combustion Institute,* Penn. State University, University Park, PA.
[39] Lutz, A.E., Kee, R.J., Grcar, J.F., Rupley, F.M., 1997, OPPDIF: A Fortran Program for Computing Opposed-flow Diffusion Flames, Report No. SAND96-8243, Sandia National Laboratories.
[40] Sung, C.J., Law, C.K., 2000, Structural sensitivity, response, and extinction of diffusion and premixed flames in oscillating counterflow. *Combustion and Flame,* **123**, 375–388.
[41] Egolfopoulos, F.N., 2000, Structure and extinction of unsteady, counterflowing, strained, non-premixed flames. *International Journal of Energy Research,* **24**, 989–1010.
[42] Lutz, A.E., Rupley, F.M., Kee, R.J., 1996, EQUIL: A CHEMKIN Implementation of STANJAN, for Computing Chemical Equilibria, Report No. SAND96-xxxx, Sandia National Laboratories.
[43] Muradoglu, M., Pope, S.B., 2002, Local time-stepping algorithm for solving the probability density function turbulence model equations. *AIAA Journal,* **40**, 1755–1763.
[44] Pantano, C., 2004, Direct simulation of non-premixed flame extinction in a methane-air jet with reduced chemistry. *Journal of Fluid Mechanics,* **514**, 231–270.
[45] Hult, J., Meier, U., Meier, W., Harvey, A., Kaminski, C.F., 2005, Experimental analysis of local flame extinction in a turbulent jet diffusion flame by high repetition 2-D laser techniques and multi-scalar measurements. *Proceedings of the Combustion Institute,* **30**, 701–709.
[46] Mastorakos, E., Baritaud, T.A., Poinsot, T.J., 1997, Numerical simulations of autoignition in turbulent mixing flows. *Combustion and Flame,* **109**, 198–223.

Appendix: Particle trajectories in physical space

Figure 18 shows the particle trajectories in physical space for the Cabra H_2/N_2 lifted flame and for the Sandia flame E, from calculations using the EMST mixing model. The top border of the plot is the free-stream boundary. When the particles from the turbulent jet approach the non-turbulent free stream, their velocity should relax rapidly towards the free stream velocity. However, from Figure 18, it may be seen that some particles shoot into the free stream with little or no relaxation of velocity, and are then reflected off the free-stream boundary (according to

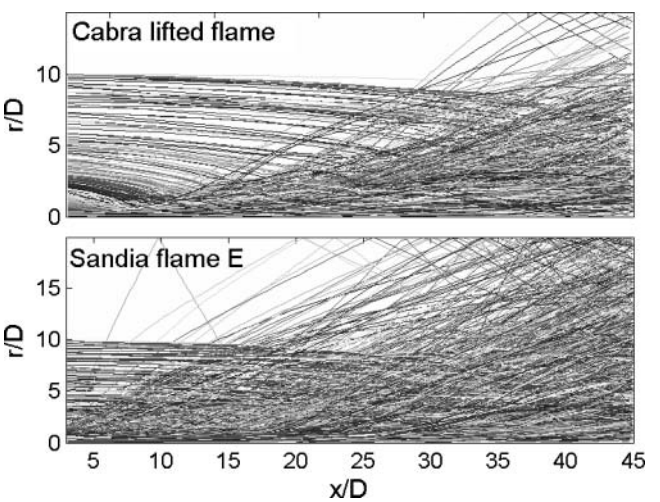

Figure 18. Particle trajectories in physical space for the Cabra H_2/N_2 lifted jet flame and for the Sandia flame E from the original turbulence frequency model.

the specified boundary condition). This non-physical behavior of the particles is not expected to occur when the conditional mean frequency Ω (Equation (7)) is used to define the time-scale in the stochastic turbulence frequency model (Equation (5)) [17]. The turbulence frequency in the turbulent region is much greater than that in the non-turbulent free stream. Ideally, if one turbulent fluid particle $\mathcal{P}$ dives into one mesh cell $\mathcal{C}$ in the laminar free stream environment, the turbulence frequency of particle $\mathcal{P}$ will be the only frequency used to determine Ω ($= C_\Omega \cdot \omega^*_\mathcal{P}$, where $\omega^*_\mathcal{P}$ is the turbulence frequency of particle $\mathcal{P}$) in cell $\mathcal{C}$ according to Equation (7). From the Langevin model Equation (4), the velocity of particle $\mathcal{P}$ will decay rapidly at rate Ω toward the free stream velocity. However, under certain circumstances, the particle $\mathcal{P}$ is not the only particle chosen to determine the conditional mean frequency Ω. In the current situation (of a cylindrical coordinate system), the initial mass of a particle is linearly proportional to the particle's radial location. Compared to the particle mass in the free stream, the mass of the particle $\mathcal{P}$ originating closer to the axis is much less. In this case, the mass-weighted mean frequency $\widetilde{\omega}$ in cell $\mathcal{C}$ is close to the mean frequency in the free stream. On the other hand, numerically the turbulence frequency for the particles in the free stream is not exactly the same, i.e., there are small fluctuations in particle turbulence frequency in the free stream. These fluctuations are caused by the Wiener process in Equation (5) and by the disturbance caused by the turbulent fluid particle $\mathcal{P}$. Assume that the maximum of the turbulence frequency in cell $\mathcal{C}$ is ω^*_{m2} when particle $\mathcal{P}$ is excluded. It may happen that ω^*_{m2} is greater than $\widetilde{\omega}$, so that the possibly massive particle with frequency ω^*_{m2} is included in the calculation of Ω. Therefore the value of Ω is much less than the desired value $C_\Omega \cdot \omega^*_\mathcal{P}$. In another words, the value of Ω is greatly under-estimated, and so is the decaying rate of the velocity of the particle $\mathcal{P}$.

In spite of the non-physical behavior of the particles described above, it should be appreciated that this behavior occurs with low probability (less than 1% of the number of tracked particles in the Cabra lifted flame, and about 5% in the Sandia flame E). They do not influence the statistics significantly. Since the particle behavior is relatively more important in this work, we try to eliminate or reduce the non-physical behavior in the following *ad hoc* way. In the above discussed case, the particle $\mathcal{P}$ should be chosen as the only particle to determine Ω, in spite of the small fluctuations of the turbulence frequency in the free stream. If we can identify this

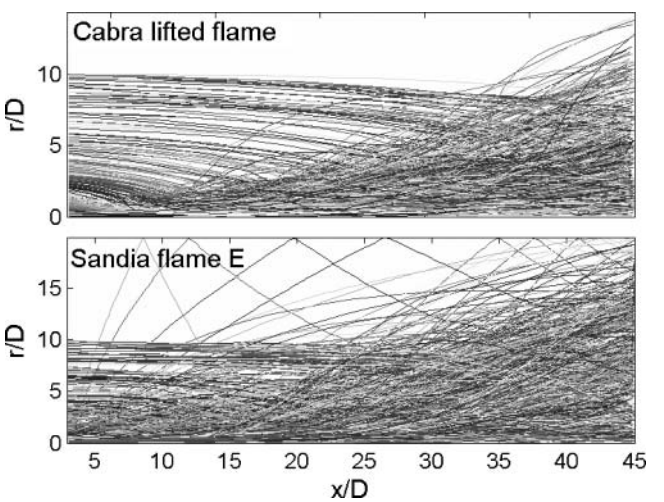

Figure 19. Particle trajectories in the physical space for the Cabra H_2/N_2 lifted jet flame and for the Sandia flame E with an *ad hoc* revision to the turbulence frequency model.

particular case, we can avoid this problem by calculating Ω using particle $\mathcal{P}$ only. We use the following criteria to identify the case. If in one grid cell, the maximum turbulence frequency $\omega^*_{\mathcal{P}}$ of a particle $\mathcal{P}$ is much greater than the Favre mean frequency $\widetilde{\omega}$ ($\omega^*_{\mathcal{P}} > c_1 \cdot \widetilde{\omega}$), and also much greater than the frequency of all other particles in the cell ($\omega^*_{\mathcal{P}} > c_2 \cdot \omega^*_{m2}$), and the mass of the particle $m^*_{\mathcal{P}}$ is much less than the average mass of the particles $\langle m \rangle$ ($m^*_{\mathcal{P}} < c_3 \cdot \langle m \rangle$), we then use particle $\mathcal{P}$ exclusively to determine Ω. The constants are chosen as $c_1 = 15$, $c_2 = 8$, and c_3=0.2. The particle trajectories in physical space obtained with this special treatment of the frequency model are shown in Figure 19. The non-physical particles disappear in the Cabra lifted flame, and the number of the non-physical particles is significantly reduced in Sandia flame E. The special treatment improves the practical performance of the turbulence frequency model to some extent. The remaining non-physical particles in the Sandia flame E shown in Figure 19 are due to the limitation of the criteria. Using a different specification of c_1, c_2, and c_3, we can eliminate the non-physical particles completely, but it also then affects the turbulence region. In this work, we use this *ad hoc* revision to reduce the number of non-physical particles. Those particles not caught by the criteria are removed from the particle subset in the discussion. This *ad hoc* revision to the frequency model does not change the statistics of the velocity and composition fields. We appreciate that the criteria does not guarantee the convergence of the method when the number of particles tends to infinity.